BL3B, 6B

Temperature-Dependent Electronic Structure Modification on an Altermagnet Candidate MnTe

S. Kimura[1,2,3], H. Watanabe[1,2], K. Yuan[2], Y. Pan[2], H. Ishida[2] and M.-H. Jung[4]
[1]*Graduate School of Frontier Biosciences, The University of Osaka, Suita 565-0871, Japan*
[2]*Department of Physics, Graduate School of Science, The University of Osaka, Toyonaka 560-0043, Japan*
[3]*Institute for Molecular Science, Okazaki 444-8585, Japan*
[4]*Department of Physics, Sogang University, Seoul 04107, Republic of Korea*

Recently, materials with antiferromagnetic and ferromagnetic characters, namely altermagnet, have attracted attention and are classified as the third magnetic material group [1]. The materials have no net magnetism, but owing to the crystal symmetry combined with the antiferromagnetic structure, there are two novel characteristics: a strong time-reversal symmetry-breaking response and the other spin-polarization phenomena typical of ferromagnets [2]. Thanks to their physical properties, the materials are considered helpful for spintronics devices [3].

One candidate for altermagnets is MnTe. The material has a Neel temperature of 307 K. The Spin-split band structure of the material has been observed with angle-resolved photoelectron spectroscopy (ARPES) [4, 5]. The experimental result is considered to be evidence of the altermagnet.

ARPES can detect the occupied electronic structure below the Fermi level (E_F), but it is impossible to observe the unoccupied state. Thus, the whole band picture cannot be probed by ARPES. On the other hand, optical conductivity (σ_1) spectra have information on the joint density of states between the occupied and unoccupied states. By the experimental characters, the combination of ARPES and σ_1 spectra provides information on the unoccupied states. Additionally, in-gap states with very low density can be observed with σ_1 spectra. Then, we measured σ_1 spectra of MnTe.

Reflection spectroscopy has been performed at BL3B from the visible to the VUV regions and at BL6B from the IR to the THz regions. The measurements were combined with the reflection spectra in the IR – visible region taken at the laboratory, and finally, whole reflectivity spectra in the photon energy of 8 meV – 40 eV were obtained. σ_1 spectra were obtained with the Kramers-Kronig analysis of the wide-range reflectivity spectra.

Figure 1 shows the temperature dependence of the σ_1 spectrum of MnTe near the energy gap at 1 eV. At 370 K, higher than T_N, a broad peak is visible at about 2.25 eV. As the temperature decreases, the peak shifts to the low energy side and narrows. The temperature dependence is almost consistent with a valence band peak observed in ARPES results [5]. However, the energy shift is about 0.2 eV, much smaller than the peak shift of 0.4 eV appearing in ARPES. To clarify the inconsistency, further band structure calculations are needed.

As shown in the inset of Fig. 1, the structural temperature change within the energy gap appearing at the low energy side is remarkable. With decreasing temperature, the intensity at around 0.5 eV decreases, while that below 0.2 eV increases. The former corresponds to the onset of the absorption edge shifting to the high energy side, which is the opposite behavior of the peak energy. This suggests that the band structure at the gap edge is modulated with decreasing temperature. The newly appeared peak below 0.2 eV suggests another localized electronic state emerges in the energy gap below T_N.

The observed characteristic temperature dependence in the σ_1 spectrum does not correspond to conventional antiferromagnetic materials; the spectral change can be regarded as originating from the band modification of altermagnetic character.

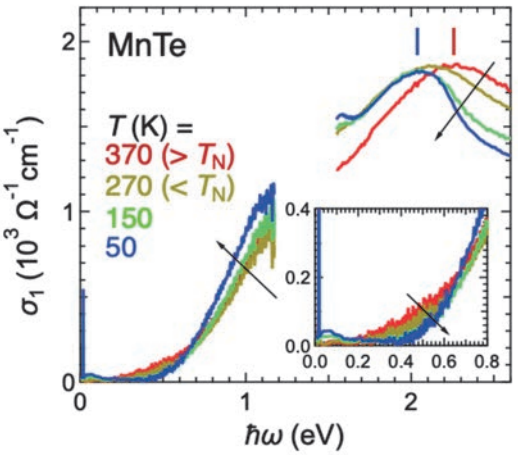

Fig. 1. Temperature-dependent optical conductivity [σ_1] spectra of MnTe near the energy gap. (Inset) The enlarged figure of the in-gap states.

[1] I. Mazin, Phys. Rev. X **12** (2022) 040002.
[2] L. Šmejkal, J. Sinova and T. Jungwirth, Phys. Rev. X **12** (2022) 040501.
[3] C. Sun and J. Linder, Phys. Rev. B **108** (2023) L140408.
[4] S. Lee *et al.*, Phys. Rev. Lett. **132** (2024) 036702.
[5] T. Osumi *et al.*, Phys. Rev. B **109** (2024) 115102.

BL3B

Low Temperature Measurements to Understand Luminescence Characteristics of Synthetic Diamond

Atsuhiro Umemoto[1]

[1]*International Center for Quantum-field Measurement Systems for Studies of the Universe and Particles (QUP), High Energy Accelerator Research Organization (KEK), Tsukuba 305-0801, Japan*

Diamond is a wide-bandgap semiconductor with unique physical properties, such as the highest Debye temperature among crystals and easy formation of optical color centers by impurity doping. Owing to these characteristics, diamond is expected to be used as a scintillating bolometer in the field of particle physics, detecting both luminescence and heat generated by charged particles. Scintillating bolometers exhibit excellent energy resolution and particle identification capabilities, which are important for rare event searches, such as dark matter search. We have been conducting research and development on both diamond scintillators and bolometers for dark matter detection. Recently, we have shown the basic characteristics of diamond scintillators by using nitrogen-doped, commercially available synthetic crystals [1]. At present, with the cooperation of Prof. Taniguchi and Miyakawa at the Research Center for Materials Nano-Architectonics, National Institute for Materials Science, synthetic diamonds with controlled dopants for optical color centers can be manufactured and used to study their luminescence properties.

During the beam time in FY2024, photoluminescence measurements were conducted on synthetic diamonds with nitrogen concentrations ranging from 1 to 200 ppm. Since scintillating bolometers operate at low temperatures, understanding their luminescence characteristics at these temperatures is very important. Figure 1 shows a comparison of the photoluminescence spectra of diamond with a nitrogen concentration of 1 ppm, measured at different temperatures. The excitation wavelength was set to λ=220 nm, which is a similar energy as the bandgap of diamond. The peak wavelength shifted from 516 nm to 569 nm when the temperature was lowered from room temperature to 7 K. While a detailed analysis has not yet been conducted, this suggests that lowering the temperature may have induced changes in the crystal structure. In any case, luminescence was observed at low temperatures, and although it was not easy to quantify the light yield, it was shown to be comparable to that at room temperature. As an interesting point from physical properties perspective, we observed that the change in the peak wavelength between low and room temperatures depends on the nitrogen concentration. The linear line shown in Fig. 2 represents predictions, but the peak wavelength might shift to shorter wavelengths at lower temperatures when the nitrogen impurity concentration exceeds 150 ppm.

The decay time constants of luminescence and other parameters show different behavior in samples with nitrogen impurity concentrations exceeding 150 ppm. Further investigations are needed to understand the luminescence characteristics at low temperatures and to determine the optimal nitrogen concentration for dark matter search.

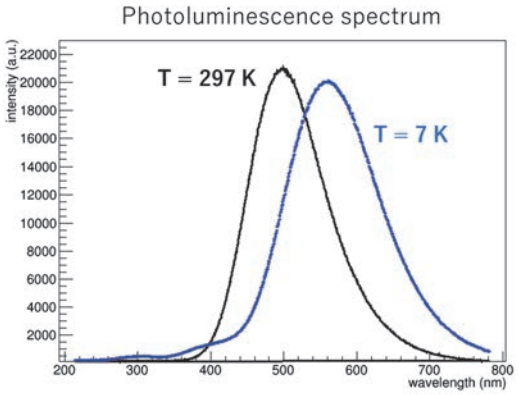

Fig. 1. Photoluminescence spectra of nitrogen-doped synthetic diamond with a nitrogen concentration of 1 ppm, measured at different sample temperatures.

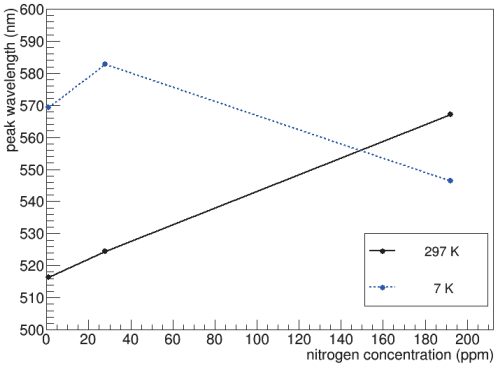

Fig. 2. The shift of the photoluminescence peak wavelength depended on the temperature. It was performed on three samples with different nitrogen concentrations.

[1] A. Umemoto *et al*., Nucl. Instrum. Methods A **1057** (2023) 168789.

BL3B

Non-Proportional Response between Scintillation Light Yield and Energy of the Incident Gamma Rays

S. Kurosawa[1,2,3], Y. Urano[2,4], C. Fujiwara[2,4] and A. Yamaji[1,2]

[1]*New Industry Creation Hatchery Center (NICHe), Tohoku University, Sendai 980-8579, Japan*
[2]*Institute for Materials Research (IMR), Tohoku University, Sendai 984-8577, Japan*
[3]*Institute of Laser Engineering, The University of Osaka, Suita, Osaka 565-0871, Japan*
[4]*Graduate School of Engineering, Tohoku University, Sendai 980-0845, Japan*

Boron neutron capture therapy (BNCT) is one of the treatments to selectively destroy cancer cells using a nuclear reaction between ^{10}B and neutrons. Although evaluation of the treatment effect in real-time is required for patient safety, the monitoring system has not been realized. The use of prompt gamma rays (478 keV) emitted by the ^{10}B(n,α)^{7}Li reaction during BNCT therapy has been proposed as this monitoring system[1], and the 478-keV gamma-ray signal should be discriminated from the background (BG) events including 511-keV gamma rays from positron and electron annihilation. Thus, scintillators are required to have an energy resolution better than 4 % (FWHM) at 511 keV.

Tl-doped $Cs_3Cu_2I_5$ (Tl:CCI) scintillator has a high light output of over 90,000 photons/MeV and a high energy resolution of 3.3% at 662 keV (FWHM), which corresponds to 3.7% at 511 keV (FWHM) [2]. Moreover, the hygroscopic nature of this material is ignorable, as even typical iodide crystals have. Thus, this material is expected to be suitable for gamma-ray detection of the BNCT clearly, if the energy resolution is improved.

Here, energy resolution is related to light yield and non-proportionality between scintillation light yield and energy of the incident gamma rays. Tl:CCI has a non-proportional response (NPR) of over 3%, where NPR is defined in [3]. Recently, NPR and energy resolution for Sr^{2+}-co-doping Tl^{+}-doped NaI have been reported to be improved [3]. Therefore, we grew Tl^{+} and Sr^{2+} co-doped CCI (Tl,Sr:CCI) crystals and evaluated their luminescence and scintillation properties.

Tl,Sr:CCI, Sr:CCI, Tl:CCI and pure CCI crystals were grown by the vertical Bridgman-Stockburger method in our laboratory, and we verified the single crystal phase and composition using several X-ray devices. Also, we have measured several optical properties such as emission and excitation wavelength, light output and NPR. The results showed Sr-dopant effect was also observed for Tl,Sr:CCI; NPR and energy resolution were improved compared to Tl:CCI

In UVSOR, we investigated several properties, especially the role of the Sr. The temperature dependence of photoluminescence excitation and emission spectra from 10 to 350 K were evaluated at UVSOR BL3B beam line.

Here, we measured excitation and emission two-dimensinal map at each temperature, and over 150K the emission and excitation wavelengths were slightly shifted for the both samples. This result suggested CCI has different emission mechanisms in the lower and higher temperature regions.

Figure 1 shows the temperature dependence of emission intensities for pure CCI and Sr:CCI, and the both data were fitted by the Arrhenius equation blow 150 K. The fitting results showed the activation energy was shifted by Sr-co-doping. This result suggested Sr^{2+} or indirect effect by the Sr^{2+} co-doping affects some trap site which is related to the non-proportionality and energy resolution.

We also measured the thermoluminescence grow curve in the BL3B beam line for the Sr-doped and Sr-free CCI. Although the results are preliminary ones, the differences are not observed clearly. These results indicated the de-excited electrons from such trap sites to ground state are relaxed by non-radiative process, or these trap sites can be located at deep level, which means de-trapping energy is expected to be over room temperature.

To analyze the details, we grew different concentration of Sr to doped with Tl:CCI and also Ca-co-dopant effect is investigated.

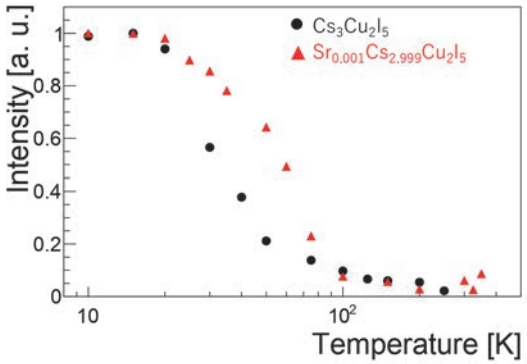

Fig. 1. Emission intensity as a function of temperature, where the intensities are normalized to 1 at 10 K.

[1] D.M. Minsky *et al.*, Appl. Radiat. Isot. **67** (2009) 179.
[2] L. Stand *et al.*, Instrum. Methods Phys. Res. A **991** (2021)164963.
[3] K. Yang *et al.,* J. Appl. Phys. **118** (2015) 213106.

BL3B

VUV Excitation Property of NIR Phosphor Eu:$CaSc_2O_4$

S. Kodama[1], T. Saito[1], I. Yanase[1] and H. Takeda[1]
[1]*Graduate school of Science and Engineering, Saitama University, 255 Shimo-Okubo, Sakura-ku, Saitama 339-8570, Japan*

Red or NIR emitting phosphors are widely used in white light-emitting diodes (LEDs) and as sensor materials such as scintillators or dosimeters. Most of the red or NIR phosphor was activated by the transition metals (particularly Cr^{3+} or Mn^{2+}) or rare earth metals exhibiting 4f-4f electron transition emission (particularly Pr^{3+}, Nd^{3+} or Yb^{3+}). Conventional red or NIR luminescence centers have several limitations, for instance, the luminescence decay is slow, and the range of excitation wavelength is narrow.

Recently, some phosphors activated by Eu^{2+} were reported to exhibited fast red or NIR emission. For example, the emission wavelengths of Eu:CaO and Eu:$Ca_3Sc_2Si_3O_{12}$ were 650 nm and 850 nm, respectively, with the faster luminescence decay than 1 μs [1,2]. Eu^{2+}-doped calcium-based materials are getting a attention as next-generational fast red or NIR phosphors. In this report, the VUV excitation property of noble NIR phosphor Eu:$CaSc_2O_4$ was investigated for the first time.

Eu:$CaSc_2O_4$ was synthesized via the high-temperature solid phase reaction from $CaCO_3$ (99.99%), Sc_2O_3 (99.99%) and Eu_2O_3 (99.99%). The starting powders are mixed in an agate mortar. The mixed powders were calcined at 1500 °C for 5 h in air. After calculating, the powders were annealed in a reducing atmosphere (N_2+H_2 gas) at 1000 °C for 5 h, and Eu^{2+}:$CaSc_2O_4$ was finally obtained [3].

The VUV-VIS-NIR photoluminescence excitation and emission spectra were measured in BL3B. The measurement temperature was 300 K. In order to cut the Eu^{3+} emission, the short-wavelength-filter (700 nm) was used in the measurement.

The photoluminescence excitation and emission spectra of Eu:$CaSc_2O_4$ is depicted in Fig. 1. The sample was excited using monochromatic photons ranging from 100 to 700 nm, and the photoluminescence emission spectra were recorded within the 550–1050 nm range. This measurement identified the Eu^{2+} emission wavelength of Eu:$CaSc_2O_4$ as 750 nm, situated in the red-NIR region. N_2+H_2 annealing at 1000 °C for 5 h should be insufficient to reduce Eu^{3+} completely into Eu^{2+}, and the Eu^{3+} 4f-4f emission was strongly observed in the same time.

The photoluminescence excitation spectra of Eu:$CaSc_2O_4$ were notably broad, spanning from 120 to 700 nm, indicating that Eu:$CaSc_2O_4$ can be excited by the entire range of VUV and visible photons. For practical applications, the excitation source for Eu:$CaSc_2O_4$ should be compatible with UV LEDs, blue LEDs, or green laser diode systems (LDSs).

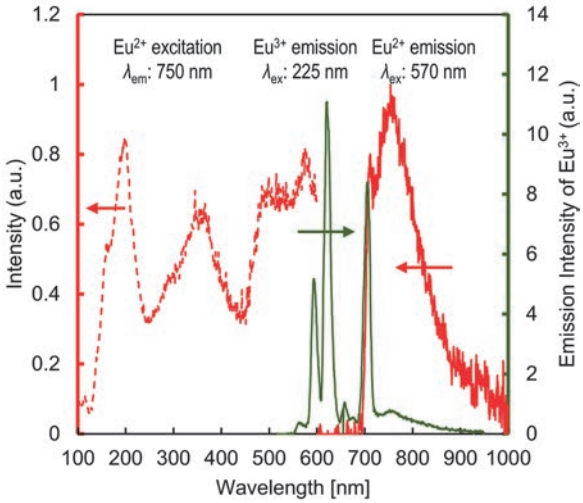

Fig. 1. Photoluminescence excitation and emission spectra of Eu:$CaSc_2O_4$.

[1] Q. Zhao *et al.*, J. Lumin. **253** (2023) 119457.
[2] I. V. Berezovskaya *et al.*, Chem. Phys. Lett. **585** (2013) 11.
[3] S. Kodama *et al.*, J. Soc. Inorg. Mater. Jpn *accepted.*

BL3B

Energy Transfer from I^- Centers to Ce^{3+} Centers in Co-Doped NaCl: I^-, Ce^{3+} Crystals

R. Oda[1] and T. Kawai[1]

[1]*Graduate School of Science, Osaka Metropolitan University, Sakai 599-8531, Japan*

Alkali halide crystals have the wide band-gap up to the vacuum ultraviolet energy region and are a suitable candidate host for doping of impurity ions. We have studied energy transfer between two kinds of impurity ions doped in alkali halide crystals from the measurements of their optical properties [1-3]. In this study, we focused on Ce^{3+} ions as acceptor ions and investigated the energy transfer from I^- Centers to Ce^{3+} Centers in co-doped NaCl:I^-, Ce^{3+} crystals.

The Ce^{3+} ions in crystals exhibit the luminescence due to the radiative transition from the lowest 5d excited level to the split 4f ground levels. The 5d -> 4f radiative transition in the Ce^{3+} ions is a dipole-allowed one with a typical decay time of about 20 ns [4]. The fast decay profiles allow us to measure a rise time due to energy transfer to the acceptor ions under single-bunch operation of UVSOR.

Figure 1 shows the luminescence and absorption spectra of co-doped NaCl:I^-, Ce^{3+} crystals at 10 K. The intense absorption and luminescence bands due to the I^- centers are observed at 6.9 eV and 5.7 eV, respectively. The luminescence band at 5.7 eV comes from one-center-type relaxed excitons, which consist of a hole localized on an iodine anion and a bound electron, that is to say, special type of bound excitons [5]. Two luminescence peaks due to the Ce^{3+} centers were observed at 3.37 eV and 3.64 eV.

Figure 2 shows decay profiles of the Ce^{3+} luminescence under the excitation on the I^- absorption band at various temperatures. Below 100 K, the Ce^{3+} luminescence exhibits the double exponential decay profiles, which have no rise time. Above 200 K, on the other hand, a rise time of a few tens of nanoseconds was observed in the decay profile of the Ce^{3+} luminescence. The rise time decreases with increasing temperature. It is difficult to believe that the slow rise time of a few tens of nanoseconds is attribute to energy transfer by the Förster-Dexter mechanism or the luminescence-reabsorption mechanism. In our previous paper [2], we have proposed the energy transfer processes through the migration of the V_K center generated from the excited I^- centers in NaCl crystals. The idea is supported by the slow rise time of a few tens of nanoseconds in the decay profile of the Ce^{3+} luminescence. The temperature dependence of the rise time indicates that the migration of the V_K center occurs by thermally activated hopping.

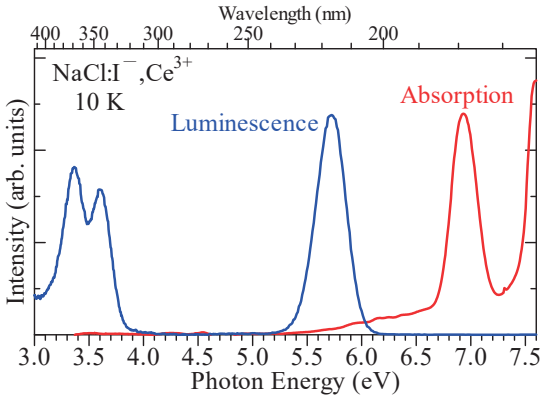

Fig. 1. Luminescence (blue) and absorption (red) spectra in co-doped NaCl:I^-, Ce^{3+} single crystals.

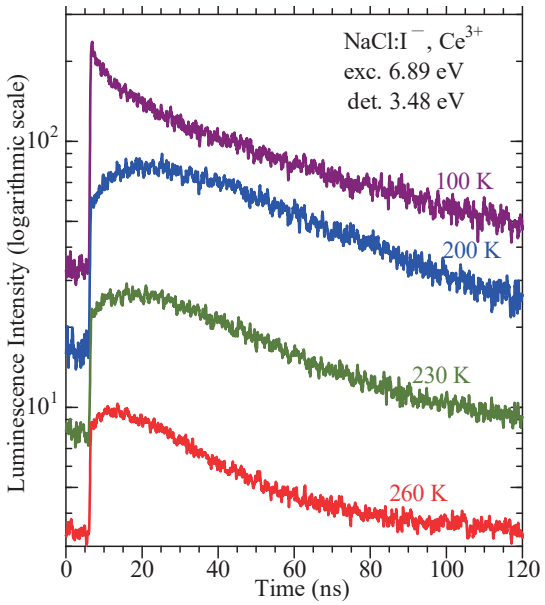

Fig. 2. Decay profiles of the Ce^{3+} luminescence under the excitation on the I^- absorption band at various temperatures.

[1] A. Iguchi, T. Kawai and K. Mizoguchi, Phys. Status Solidi C **13** (2015) 85.
[2] O. Yagi, T. Kawai and K. Mizoguchi, J. Lumin. **226** (2020) 117359.
[3] R. Oda and T. Kawai, UVSOR Activity Report **51** (2024) 80.
[4] Y. Yokota *et al*., Radiat. Meas. **45** (2010) 472.
[5] I. Akimoto, M. Shimozato and K. Kan'no, Phys. Status Solidi C **6** (2009) 342.

BL3B

Investigation of Charge Transfer Energies in Eu^{3+}-Doped Layered Mixed-Anion Phosphor by VUV Spectroscopy

H. Miyata[1] and J. Ueda[1]
[1]*Japan Advanced Institute of Science and Technology, Nomi 923-1292, Japan*

Persistent phosphors are luminescent materials that emit light for a long duration after the excitation source is turned off. They are widely used in many applications such as luminous paints in the dark for hazard signboards and road markers and luminescent markers for in vivo imaging. Persistent luminescence originates from the temporary trapping of the electrons or holes, generated with light absorption, by crystalline defects. The trapped electrons or holes are thermally released and transferred back to the luminescent center.

So far, aluminate and silicate compounds such as $SrAl_2O_4$:Eu^{2+}-Dy^{3+} [1] and $Sr_2MgSi_2O_7$:Eu^{2+}-Dy^{3+} have been widely used as practical persistent phosphors. In contrast, oxides including other oxoanion (CO_3^{2-}, NO_3^- and etc.) and non-oxides are still an unexplored material group for persistent phosphors and have the potential to show excellent persistent luminescent properties. Existing persistent phosphors have mostly shown blue and green luminescence. Therefore, there is a need to develop high-performance red persistent phosphors. Eu^{3+} is a promising candidate as a red emitting central ion. In addition, long afterglow properties have been reported for Eu^{3+}-doped phosphors in Y_2O_2S:Eu^{3+}-Ti-Mg.

In Eu^{3+}-doped persistent phosphors, the (de)trapping carriers are holes. Thus, the holes migrate in the valence band (VB) after charge transfer excitation and are trapped by crystalline defects and metal ions.[2] Therefore, understanding charge transfer (CT) behavior in Eu^{3+}-doped phosphors is essential for the development of persistent phosphors. In this study, we focus on Eu^{3+}-doped $La_2O_2CO_3$ reported by Masui and Imanaka [3]. Here, we prepared another polymorph of Eu^{3+}-doped $La_2O_2CO_3$ and discussed its charge transfer behavior from VUV PLE spectra.

Photoluminescence excitation (PLE) spectra of Eu^{3+} doped $La_2O_2CO_3$ at 10 K are shown in Fig. 1. PLE spectra were measured with monitoring Eu^{3+} $^5D_0$–$^7F_0$ emission. In the PLE spectra, two broad PLE bands are observed around 175 nm and 192 nm. The PLE band at 192 nm is attributed to the CT band of Eu^{3+}, and the PLE peak at 175 nm is attributed to the host-exciton formation. The E_g is calculated to be 6.98 eV using the obtained E_{ex} (192 nm). The CT bands were well-fitted by two Gaussian functions. Since $La_2O_2CO_3$ is a mixed anion compound, charge transfers derived from the two anions O^{2-} and CO_3^{2-} are possible. The CT energy (E_{CT}) of single anion compounds La_2O_3:Eu were reported to be 4.27 eV [4], and $Eu_2(CO_3)_3$ was estimated to be 5.30 eV from the PLE spectrum. Based on the obtained E_{CT}, a stacked vacuum referred binding energy (VRBE) diagram are prepared as shown in Fig. 2. According to the VRBE diagram, the low-energy CT band is attributed to O^{2-} and the high-energy CT band to CO_3^{2-}. By mixing with carbonate anion, the oxide can lower the valence band energy. Based on the valence band engineering by oxoanion doping, the hole-detrapping persistent phosphors will be developed in the future.

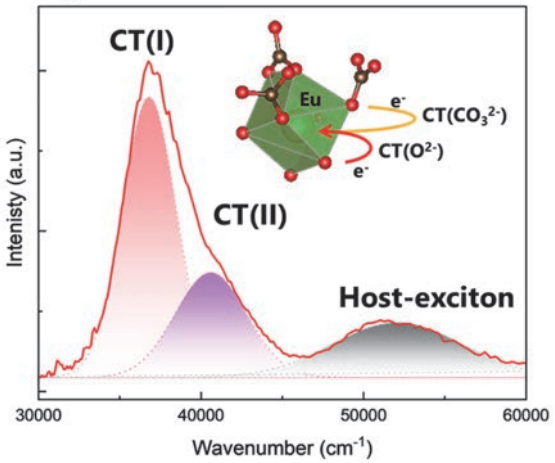

Fig. 1. PLE spectra of $La_2O_2CO_3$:Eu and crystal structure of $La_2O_2CO_3$ around La site.

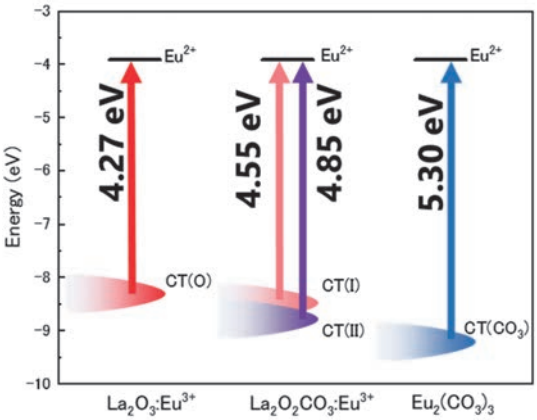

Fig. 2. Energy diagram of $Eu3^+$ charge transfer state and valence band top of La_2O_3, $La_2O_2CO_3$, $Eu_2(CO_3)_2$.

[1] T. Matsuzawa *et al.*, J. Electrochem. Soc. **143** (1996) 2670.
[2] J. Ueda, Bull. Chem. Soc. Japan **94** 2 (2021) 2807.
[3] K. Koyabu, N. Imanaka, *et al.*, J. Alloys Compd. **408–412** (2006) 867.
[4] Linkang Yu *et al.*, J. Lumin. **229** (2021) 117663.

BL3B

Effect of Ag-Doped Phosphate Glass for Radiophotoluminescence Dosimeter

J.Y. Cho[1], E.J. Choi[1], D.W. Jeong[1], N.D. Ton[1] and H.J. Kim[1]
[1]*Department of Physics, Kyungpook National University, Daegu 41566, Republic of Korea*

The release of large quantities of radioactive material during nuclear disasters such as Fukushima and Chernobyl has highlighted the critical importance of accurate radiation dosimetry. Reliable dose measurement is essential for ensuring radiation safety, assessing long-term health risks, and implementing appropriate protective measures. Traditional dosimeters such as Metal-Oxide-Semiconductor Field-Effect Transistor (MOSFET) dosimeters and thermoluminescence dosimeters (TLDs) are widely used due to their sensitivity and reusability. However, TLDs suffer from significant drawbacks, including high-temperature readouts, signal fading over time, and limited reproducibility. These limitations emphasize the need for alternative dosimetry technologies with improved performance and reliability. Radiophotoluminescence (RPL) glass dosimeters have emerged as a promising solution, offering excellent signal stability, dose linearity, and long-term reproducibility. In particular, the commercial GD-450 dosimeter, based on silver-doped phosphate glass, has demonstrated robust performance in both personal and environmental radiation monitoring.

Building on the strengths of existing RPL technologies, this study focuses on the development of enhanced RPL glass dosimeters through compositional engineering. Specifically, silver-doped phosphate glasses were synthesized using a variety of glass-modifying oxides to tailor their structural and luminescent properties. Glass modifiers play a crucial role in adjusting physical and optical characteristics by introducing non-bridging oxygens that alter the glass network. Drawing from previous research, including studies by Miyamoto *et al*. and Yoshida *et al*. [1, 2], which clarified the emission mechanisms and improved the thermal stability of silver-doped glasses, we aimed to further optimize RPL performance. By comparing the newly developed glasses with the commercial GD-450, this study investigates improvements in sensitivity and dose linearity, with the ultimate goal of advancing RPL dosimetry technologies for broader and more demanding applications.

The PLAN glasses were fabricated two way using conventional melting quenching method at atmospheric environment and induction melting quenching method at nitrogen enviroment in following composition: ($75.6P_2O_5$-$18.2Li_2$-$2.6Al_2O_3$-$2.6NaBr$-$1.0Ag_3PO_4$, PLAN). Fabricated glasses evaluated their photoluminescence (PL) at room temperature using BL3B beam line.

Fig. 1. PLAN:Ag glasses.

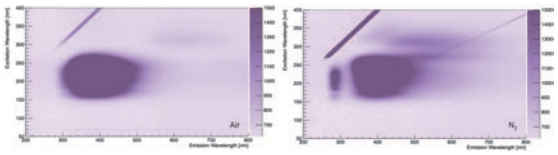

Fig. 2. The excitation and emission 2D scanning spectra.

Figure 1 shows fabricated glasses, and photoluminescence excitation and emission (2D scanning) spectra for these samples were displayed in Fig. 2. In the emission spectra, the emission around excitation wavelength between 150-275 nm is host emission of PLAN glasses and 300-350 nm is RPL emission. However, the RPL emission from nitrogen environment fabricated glasses slightly blue shift is observed. Also, emission from 275-300 nm is observed only nitrogen fabricated glasses.

This results indicated environment during fabrication is important to enhanced its luminescence and transparency.

[1] M. Yoshida *et al*., Radiat. Meas. **45** (2010) 890.
[2] Y. Miyamoto *et al*., Radiat. Meas. **45** (2010) 546.

III-2

BL3B

Valence Fragmentation Dynamics of a Promising Low Global Warming Etching Gas CF_3CHCF_2

Tran T. Nguyen[1], T. Hayashi[1], H. Iwayama[2] and K. Ishikawa[1]
[1]*Nagoya University, Furo, Chikusa, Nagoya 464-8601, Japan*
[2]*UVSOR Synchrotron Facility, Institute for Molecular Science, Okazaki 444-8585, Japan*

The semiconductor industry faces significant challenges in etching high-aspect-ratio (HAR) structures for fabrication of 3D flash memory. Traditional reactive ion etching (RIE) processes struggle with issues on aspect-ratio-dependent etching and require precise control to maintain high-quality profiles [1]. Hydrofluorocarbons (HFCs) and perfluorocarbons (PFCs) gases are widely used in the HAR etching processes; despite their impact on global warming. To address these environmental concerns, the industry is exploring alternative gas chemistries and process techniques, including low-GWP fluorocarbons [2, 3].

In this study, we have investigated dissociation of C_3HF_5 by the PEPICO (Photo Electron Photo Ion CO incidence) technique using synchrotron radiation [4]. Identifying key dissociative fragments provided valuable insights for optimization of the etching results and minimization of their environmental impact.

The PEPICO experiments were conducted at the UVSOR facility in Japan, utilizing a 2.5 m off-plane Eagle-type monochromator to generate tunable vacuum ultraviolet (VUV) light in the energy range of 10-26 eV. C_3HF_5 gas was introduced into a high-vacuum chamber and irradiated with the VUV light. A time-of-flight mass spectrometer was employed to detect the resulting fragment ions. By analyzing the ion yield curves as a function of photon energy, appearance energies were determined, providing valuable insights into the dissociation pathways and energetics of C_3HF_5 molecules.

The dissociative photoionization of C_3HF_5 was systematically characterized across 10–26 eV using PEPICO spectroscopy. At 20 eV, the mass spectrum revealed dominant fragment ions such as $C_3HF_4^+$ and $C_3F_4^+$, alongside significant contributions from CF_3^+ and $C_2F_3^+$. The parent ion $C_3HF_5^+$ persisted at this energy, while weaker signals for smaller fragments (e.g., $C_3F_3^+$, $C_2F_2^+$) suggested secondary dissociation pathways. Figure 1 shows a breakdown diagram constructed from the ion yield curves. The breakdown diagram illustrated a photon-energy-dependent evolution in fragmentation: below 14 eV, the parent ion dominated (~80% abundance), with minor $C_3F_5^+$ (~20%) from H loss. Above 14 eV, a sharp transition occurred, with $C_3HF_4^+$ (F loss) and $C_3F_4^+$ (HF loss) emerging as primary products, collectively contributing ~54% of the ion yield by 15.5 eV. Notably, CF_3^+ became increasingly prominent above 15.2 eV, reaching ~25% abundance at 19–26 eV. Appearance energies (AEs), derived from ion yield thresholds, confirmed sequential fragmentation: the parent ion $C_3HF_5^+$ originated at 10.6 ± 0.06 eV, followed by $C_3F_5^+$ (10.7 ± 0.03 eV). $C_3HF_4^+$ exhibited dual pathways (13.7 ± 0.02 eV and 14.2 ± 0.04 eV), attributed to distinct C–F bond cleavages in CF_3 and CF_2 groups, while $C_3F_4^+$ showed similar dual thresholds (13.5 ± 0.02 eV and 14.5 ± 0.03 eV). Secondary fragments (e.g., CF^+) emerged above 17.9 eV but contributed minimally (<3%), underscoring the dominance of primary dissociation channels.

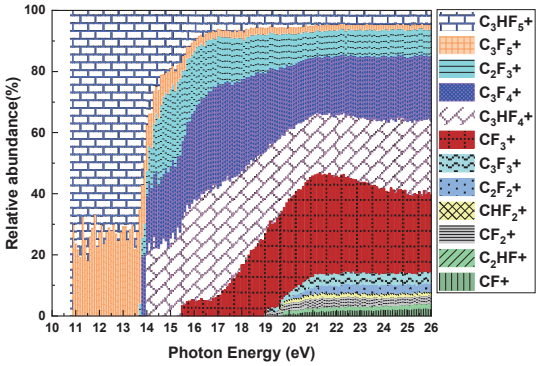

Fig. 1. Relative abundance curves of the fragment ions produced from the photoionization of C_3HF_5.

C_3HF_5 fragmentation balances fluorine-rich (CF_3^+, $C_3F_4^+$) and hydrogen-containing ($C_3HF_4^+$) species, critical for SiO_2/SiN etching. Fluorine radicals enhance SiO_2 etching, while hydrogen promotes polymer deposition for selectivity. Below 14 eV, minimal fragmentation favors parent ions; higher energies (>15 eV) optimize reactive fragment yields. The AE data align with plasma conditions (1–5 eV electron energies), suggesting C_3HF_5 efficiency in generating key etching species at low thresholds.

C_3HF_5 low-energy fragmentation pathways, characterized by PEPICO, validate its suitability as an eco-friendly etching gas. Optimizing photon energy controls reactive species, advancing high-aspect-ratio etching in semiconductor manufacturing. This study provides a framework for designing next-generation low-GWP etching gases.

[1] S. N. Hsiao *et al.*, Appl. Surf. Sci. **542** (2021) 148439.
[2] T. N. Tran *et al.*, Appl. Surf. Sci. **684** (2025) 161815.
[3] C. Abe *et al.*, Jpn. J. Appl. Phys. **63** (2024) 06SP10.
[4] T. N. Tran, *et al.*, Sci. Rep. **15** (2025) 9507.

BL3B, 5B, 7B

Delayed Fragmentation of Ethanol Molecules Induced by Photoionization

T. Nakao[1], T. Kaneyasu[2,3], H. Iwayama[3], T. Yanagawaya[4] and T. Majima[1]
[1]*Department of Nuclear Engineering, Kyoto University, Kyoto 615-8540, Japan*
[2]*SAGA Light Source, Tosu 841-0005, Japan*
[3]*Institute for Molecular Science, Okazaki 444-8585, Japan*
[4]*Faculty of Engineering, Kyoto University, Kyoto 606-8501, Japan*

Characterizing the intermediate states of ionized and excited molecules before dissociation is a key to understanding the fragmentation mechanism. Valuable insights into the intermediate states can be obtained through an analysis of the delayed fragmentation processes. We investigated the delayed fragmentation from various singly charged intermediate ions by coincidence measurement of product ions and neutral fragments using time-of-flight (TOF) mass spectrometry [1]. We have observed delayed fragmentation from nucleobase (adenine, guanine, cytosine, thymine, and uracil) and alcohol (ethanol, 1-propanol, and 2-propanol) molecules induced by MeV-energy fast ion collisions so far. The results indicated that large degrees of freedom are essential to the delayed fragmentation from singly charged intermediate ions. However, due to the complexity of fast-ion-induced processes, the characteristics of intermediate ions are not fully understood. In this study, we carried out photoionization experiments in the vacuum ultraviolet (VUV) region.

The experiments were performed at the bending magnet beamlines BL3B, BL5B, and BL7B of the UVSOR III facility. The main measurement was performed at BL7B after the test experiments at BL3B and BL5B. Monochromatic VUV light in the range of 13.0–23.0 eV photon energy was delivered to the experimental apparatus equipped with a TOF mass spectrometer. Effusive molecular beam of ethanol was used as the target. Fragments were detected with a microchannel plate (MCP) detector and recorded in event-by-event mode by a multichannel scaler.

Figure 1 shows TOF correlation spectra of the two fragments measured at a photon energy of 18.0 eV. Delayed fragmentation processes from singly charged intermediate ions are clearly visible as long diagonal tails extend from spots. Note that in this experiment neutral fragments are detectable in the delayed fragmentation, although the detection efficiency of them is relatively low due to the insufficient impact energy to be detected by the MCP. This is because they are generated during the extraction from the ionization region to the drift tube.

The delayed fragmentation channels were identified by comparing the experimental results and the calculated curves shown on the right side of Fig.1. The numbers in the figure correspond to the following channels: (1) $C_2H_5O^+ \rightarrow CHO^+ + CH_4$, (2) $C_2H_5O^+ \rightarrow C_2H_3^+ + H_2O$, (3) $C_2H_5O^+ \rightarrow H_3O^+ + C_2H_2$, and (4) $C_2H_3O^+ \rightarrow CH_3^+ + CO$. These pathways are the same as the MeV-energy fast ion collisions. The delayed fragmentation events at the tails in Fig. 1 indicate that the intermediate ions remain undissociated for submicroseconds.

The photon energy dependence of each delayed fragmentation channel was investigated, except for channel 2 because of the low statistics. Channel 1 and channel 3 show a similar energy dependence: the tail appears rapidly at about 14 eV. For channel 3, the tail appears gradually at about 17 eV. Since the vertical ionization potential of ethanol is about 10.6 eV [2], the results indicate that these delayed fragmentation processes can be induced with an internal energy of a few eV. These threshold energies are consistent with the preliminary results of the quantum chemical calculations we performed.

The photon energy dependence of the decay curve of the intermediate ion $C_2H_5O^+$ on channel 3 was also obtained by analyzing TOF spectra. The decay curve shows a $1/t$ dependence above 15 eV. This result indicates that the internal energy transferred to vibrational excitation is the key to delayed fragmentation.

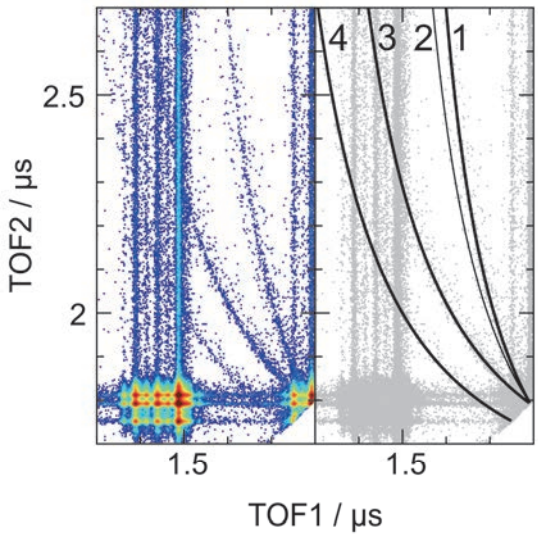

Fig. 1. TOF correlation spectra at 18.0 eV. Four delayed fragmentation channels were determined by comparing the experimental results (left) and the calculated curves (right). The numbers correspond to each dissociation channel.

[1] T. Nakao *et al.*, J. Chem. Phys. **161** (2024) 054302.
[2] P. Linusson *et al.*, Phys. Rev. A **80** (2009) 032516.

BL3B

Evaluation of Properties of Inner Region of Zinc Aluminate Thin Film for Ultra violet Emission

H. Kominami[1,2,3], J. Kamikawa[1], T. Sadamori[1], D. Takeya[1], M. Yasuda[1], N. Yoshimura[1], K. Kamiya[2], H. Nagao[2], K. Murata[2], K. Yamaguchi[2] and S. Kurosawa[4,5]

[1]*Graduate School of Integrated Science and Technology, Shizuoka University,*
[2]*Faculty of Engineering, Shizuoka University,*
[3]*Graduate School of Science and Technology, Shizuoka University,*
[1~3]*3-5-1 Johoku, Chuo-ku, Hamamatsu 432-8651 Japan*
[4]*New Industry Creation Hatchery Center (NICHe), Tohoku University 6-6-10 Aza-Aoba, Aramaki, Aoba-ku, Sendai, Miyagi 980-8579, Japan*
[5]*Faculty of science, Yamagata University, 1-4-12, Kojirakawa-machi, Yamagata 990-8560, Japan*

In the fields of sterilization and water purification, conventional sterilization methods using chemicals and heat are concerned about the effects of deterioration, toxicity to the human body, and the effects of resistant bacteria. For this reason, sterilization methods using ultraviolet light are becoming more widespread. It is said that ultraviolet light around 260 nm has the strongest effect. Mercury lamps and other devices are used as ultraviolet light sources for sterilization, but their use is concerned from the perspective of environmental impact. Under these circumstances, we aim to develop a new ultraviolet light-emitting device for sterilization that is highly efficient, low-cost, and has a low environmental impact. As one of these devices, we focused on a device that uses $ZnAl_2O_4$, which emits deep ultraviolet light around 250 nm when excited by electron beams, as the emitting layer. We are currently working on the fabrication of a double-insulated electroluminescence (EL) lamp, which is one of the solid-state display elements. There are many challenges in developing this device, such as improving the sterilization ability, controlling the voltage applied to the emitting layer, and fabricating an ultraviolet-transparent electrode. In particular, it is necessary to know the dielectric constant of the emitting layer to control the applied voltage, but the dielectric constant of the emitting layer $ZnAl_2O_4$ is currently unknown. Therefore, we attempted to obtain the refractive index from the fluctuation of the transmittance spectrum of the emitting layer, and from that, to obtain the dielectric constant.

On a c-plane sapphire substrate (c-Al_2O_3), he deposited about 300 nm of ZnO by magnetron sputtering, and on top of that he deposited about 25 nm of Al_2O_3 as a cap layer. After sputtering, he fabricated $ZnAl_2O_4$ thin films by annealing (990°C, 50 hours) under atmospheric conditions in a muffle furnace and by thermal diffusion. In addition, the thin film surface of the prepared sample was etched using hydrochloric acid to expose the inside of the film, and its characteristics were evaluated using cathodo-luminescence (CL), thin film X-ray diffraction measurement (XRD), analytical FE-SEM, and transmission.

The transmission spectrum of the sample etched for 0 to 300 minutes (0 to 450 nm) is shown in Fig. 1. Interference was observed at wavelengths of 180 to 350 nm. Here, the wavelengths of the peaks of the spectrum fluctuation are λ1, λ3, and λ5 from the short wavelength side, and the wavelengths of the valleys are λ2 and λ4, and we tried to derive the refractive index from these wavelengths.

From the cathodoluminescence measurement, the emitting layer region is calculated to be about 1200 nm. Therefore, calculations were performed assuming that Zn diffusion is 1000 and 1400 nm. As a result, when the diffusion length is assumed to be 1000 nm, the refractive index is about 4 to 5. On the other hand, when the diffusion length is assumed to be 1400 nm, the refractive index is about 3. From past research, it is thought that a layer of Zn diffused into the sapphire substrate is formed inside the thin film. In addition, the dielectric constant of the sapphire substrate is 9, and the refractive index is converted to about 3 without considering the extinction coefficient. From these facts, it is considered appropriate to assume that the refractive index after 450 nm etching is about 3, and that the Zn diffusion length is 1400 nm. In addition, because a good $ZnAl_2O_4$ layer is formed from the surface to about 400 nm, the refractive index is thought to be about 1.9 to 2.3, and the dielectric constant is thought to be about 3.6 to 5.3.

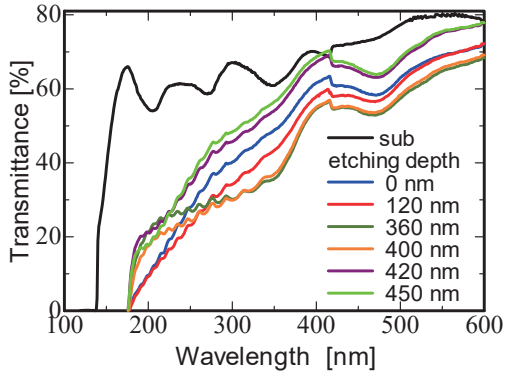

Fig. 1. Transmission spectra of etched $ZnAl_2O_4$ thin films.